Inorganic Chemistry

Article

pubs.acs.org/IC

Ab Initio Study of the Adsorption of Small Molecules on Metal–Organic Frameworks with Oxo-centered Trimetallic Building Units: The Role of the Undercoordinated Metal Ion

Andreas Mavrandonakis,*,†,∇ Konstantinos D. Vogiatzis,‡,§,∇ A. Daniel Boese,∥ Karin Fink,§ Thomas Heine,† and Wim Klopper‡,§

†Department of Physics and Earth Science, Jacobs University Bremen, Campus Ring 1, 28759 Bremen, Germany

‡Institute of Physical Chemistry, Karlsruhe Institute of Technology (KIT), Fritz-Haber-Weg 2, D-76131 Karlsruhe, Germany

§Institute of Nanotechnology, Karlsruhe Institute of Technology (KIT), Hermann-von-Helmholtz-Platz 1, D-76344 Eggenstein-Leopoldshafen, Germany

∥Department of Chemistry, University of Graz, Heinrichstraße 28/IV, 8010 Graz, Austria

Supporting Information

ABSTRACT: The interactions of H_2, CO, CO_2, and H_2O with the undercoordinated metal centers of the trimetallic oxo-centered $M_3^{III}(\mu_3\text{-O})(X)(COO)_6$ moiety are studied by means of wave function and density functional theory. This trimetallic oxo-centered cluster is a common building unit in several metal–organic frameworks (MOFs) such as MIL-100, MIL-101, and MIL-127 (also referred to as soc-MOF). A combinatorial computational screening is performed for a large variety of trimetallic oxo-centered units $M_3^{III}O$ ($M = Al^{3+}, Sc^{3+}, V^{3+}, Cr^{3+}, Fe^{3+}, Ga^{3+}, Rh^{3+}, In^{3+}, Ir^{3+}$) interacting with H_2O, H_2, CO, and CO_2. The screening addresses interaction energies, adsorption enthalpies, and vibrational properties. The results show that the Rh and Ir analogues are very promising materials for gas storage and separations.

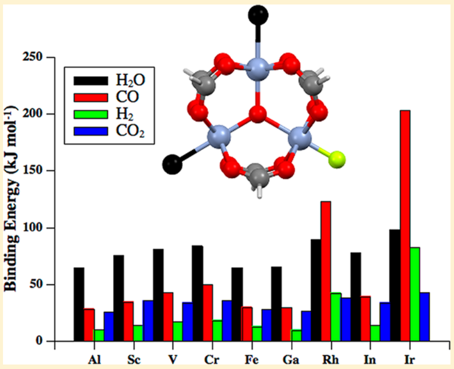

INTRODUCTION

Porous coordination materials such as metal/covalent organic frameworks (MOFs/COFs) have attracted considerable interest for their potential use in catalysis, gas storage, and gas separation.[1−4] MOFs are very promising materials, because of their structural diversity. They are constructed by linking metal oxide connectors to organic linkers. Yaghi et al. introduced the concept of reticular chemistry, according to which it is possible to tailor a desired MOF by combining the appropriate metal oxide and the organic linker.[5] A vast number of different MOFs may be constructed by using all possible combinations of metal oxide connectors and organic linkers.

Of particular interest are dihydrogen and carbon dioxide, because of their environmental and economic importance. Dihydrogen is considered to be the most promising energy carrier for the substitution of fast diminishing liquid fuel resources in mobile applications.[6] In particular, H_2 is a fully renewable energy source, environmentally friendly, nontoxic, and suitable as an automobile fuel. It has high gravimetric energy density and its combustion produces only water and no pollutant exhaust gases such as CO, CO_2, and nitrogen oxides, contrary to the combustion of conventional fossil fuels. Carbon dioxide emissions from burning of fossil fuels are considered to have the biggest contribution to the greenhouse effect and subsequently to climate change. Of significant importance is carbon dioxide capture and sequestration (CCS). There is great interest in selective pre- and post-combustion capture of CO_2.[7] A large number of MOFs are reported to have sizable H_2 and CO_2 storage abilities.[8]

MOFs can enhance the H_2 and CO_2 storage capacity by (i) incorporation of exposed metal sites either on the metal connector or by using organic linkers doped with metal cations and (ii) increase of the surface area.[3,9] The first approach enhances significantly the isosteric heat of adsorption and the gas uptake at low pressures while the second one enhances these at intermediate and high pressures. In the present work, we focus on the first approach. It has been shown recently that better selectivities for CO_2 capture were achieved by using MOFs with exposed metal sites.[10] These active sites show a strong selectivity for dihydrogen isotopologues and can thus be used for hydrogen isotope separation.[11,12]

The key point in creating MOFs with exposed metal sites is the "activation" procedure, that is, the successful removal of any axial ligands while retaining structure integrity and porosity. After the synthetic procedure, the metal sites are occupied by solvent molecules, such as water, *N*,*N*-dimethylformamide (DMF), *N*,*N*-diethylformamide (DEF), or dimethyl sulfoxide

Received: March 26, 2015
Published: August 7, 2015

DOI: 10.1021/acs.inorgchem.5b00689
Inorg. Chem. 2015, 54, 8251−8263

(DMSO). Several approaches are used for the removal of the guest molecules and the creation of coordinatively unsaturated metal sites.[13]

A common procedure that is followed to prove the existence of the open metal sites is the use of probe molecules, most commonly carbon monoxide. CO is a weak base and readily interacts with MOFs with Lewis-acid open metal sites. CO shows a distinctive infrared (IR) absorption band from the fundamental C−O stretching mode when it interacts through its carbon atom with the metal cations. The frequency is shifted to larger or smaller values, with respect to the free gaseous molecule, depending on the binding strength, the oxidation state, and the coordination environment of the metal cation. This allows identification of the formation of open metal sites or possible defects in MOFs. In a recent work, experiments and simulations of IR spectroscopy were used to prove the existence of irregular Cu^I sites in the $Cu^{II}_3(BTC)_2$ MOF.[14] Similarly, IR spectroscopy with CO was used to investigate the acidity of the Al^{3+} and Cr^{3+} sites of MIL-100.[15] Moreover, thermodynamic properties of the framework−gas interactions, that is, enthalpies and entropies of adsorption, are available via variable-temperature infrared (VTIR) experiments,[16] thus making the vibrational properties of the adsorbed species even more important.

The use of computer simulations has been proven a useful tool for the explanation of the mechanical, electronic, and adsorption properties of various porous materials.[17] Moreover, they allow the prediction of the properties of hypothetical MOFs and thus give directions toward experimental synthesis. Several works have been published where the authors screen a variety of metal connectors for H_2 and CO_2 binding by using computational techniques, such as wave-function-based theory (WFT), density functional theory (DFT), and Grand Canonical Monte Carlo (GCMC) methods. The WFT and DFT calculations can provide a quantitative description of the binding mechanism and interactions while GCMC can simulate adsorption isotherms and calculate enthalpies at various thermodynamic conditions. Typically, the GCMC methods employ empirical force fields that are based on experimental or WFT/DFT data. Several force fields have been developed in order to study these systems.[18,19]

Koh et al. reported a DFT computational screening of 36 metal-substituted variants in the M-HKUST-1 and M-CPO-27 (known also as MOF-74, M_2(dobdc), or M_2-dhtp) MOFs for their CO_2 adsorption enthalpies.[20] The M-HKUST-1 MOF (M = Cu) is based on bimetallic paddle-wheel units, which are interconnected via the tritopic benzene-tricarboxylate ligand into a framework of a **tbo** topology. The M-CPO-27 (M = Mg, Fe, Co, Ni, Zn) has one-dimensional (1-D) pores with a honeycomb-like structure and consists of metal atoms connected to 2,5-dihydroxyterephthalic acid (dhtp). In both MOFs, the solvent can be removed by thermal treatment, resulting in an activated and stable framework with coordinatively unsaturated metal centers. The authors identified several compounds that show the desired adsorption enthalpies within the range of -40 kJ mol^{-1} to -75 kJ mol^{-1}. Similarly, Park et al. reported that the CO_2 binding affinity can be tuned by changing the metal composition, and significantly increased it for the case of Ti and V.[21] In a recent combined experimental and computational work, the CO_2 binding strength on several variants of the M-CPO-27 MOF was presented and it has been concluded that the binding order can be explained by the effective charge of the metal ions.[22] All these works conclude that dispersion and electrostatic interactions are crucial for the binding. However, there are significant contributions from forward donation of the lone electron pair of CO_2 to the unoccupied *d*-orbitals of the transition metals, especially for the cases of Ti and V. In another work, DFT calculations were used to show that the not-yet-synthesized V-CPO-27 analogue is a more promising material for N_2 separation from CH_4 than Fe-CPO-27.[23] The authors calculated very strong interactions of the V sites with dinitrogen, whereas interactions with methane were significantly weaker. Fe-CPO-27 did not show stronger interactions for N_2 than for CH_4, thus making the vanadium analogue a promising material. An analysis of the natural bonding orbitals showed that the strong interactions of V(II) with N_2 are due to the significant π back-donation from the metal to dinitrogen, whereas no back-donation occurs for the CH_4 molecule or the Fe(II) site.

In a recent work, Sumida et al. performed a combined experimental and computational study on the hydrogen storage properties of M^{II}-BTT (BTT^{3-} = 1,3,5-benzenetristetrazolate) MOFs.[24] By using DFT calculations and VTIR measurements, these authors were able to determine the thermodynamic parameters for the H_2 adsorption in Mn, Fe, and Cu analogues. As a next step, the DFT calculations suggested that the Zn analogue would have better H_2 binding affinities. Moreover, they showed that the central metal ion plays an important role, and, by replacing it with more diffuse ions, the H_2 binding on the metal center was enhanced.

Bak et al. performed a computational screening on frameworks possessing a paddle-wheel connector with all 3*d* transition metals.[25] Using DFT calculations, they predicted strong H_2 interactions of ∼20 kJ mol^{-1} for the nonmagnetic Co_2 and Zn_2 paddle wheels, whereas strong binding is hindered for the early metals from Sc to Cr, because of covalent metal−metal bonds, and for Mn and Fe, because of the strong ferromagnetic coupling. Canepa et al. performed a high-throughput screening with DFT calculations on the adsorption of small molecules on the M-CPO-27 framework.[26,27] They extended their study to all possible metal compositions by including 25 different metal atoms. They studied the interactions with H_2, CH_4, CO_2, and H_2O. They found that metal species at the left of the periodic table are less effective in capturing CO_2, displaying a larger affinity for H_2O. However, the noble metals such as Rh, Pd, Os, Ir, and Pt show increased interactions with CO_2, while the affinity for water was smaller. This is significant for applications in carbon dioxide capture, where the humidity issue plays an important role. In almost all cases, the metals show interaction energies of ∼20 kJ mol^{-1} with H_2. Lee et al., in a similar study, identified the Cu analogue as suitable for capturing CO_2 from flue gas under humid conditions.[27] Moreover, they suggested the Mn analogue as promising candidate for adsorption of toxic gases and flue gas impurities, such as H_2S, SO_2, and NH_3. Their conclusions were based on DFT calculations.

Although some of the metal-substituted analogues are still hypothetical materials and have not been synthesized, these works emphasize the importance of calculations in analyzing the mechanism of interactions between small molecules and the open metal sites. As a next step, the calculations may provide useful directions to experimentalists toward promising compounds with the desired storage properties. In all of the above-mentioned studies, the authors were concentrating on synthesizing and studying the adsorption of gases on MOFs with activated (or under-coordinated) metal sites.

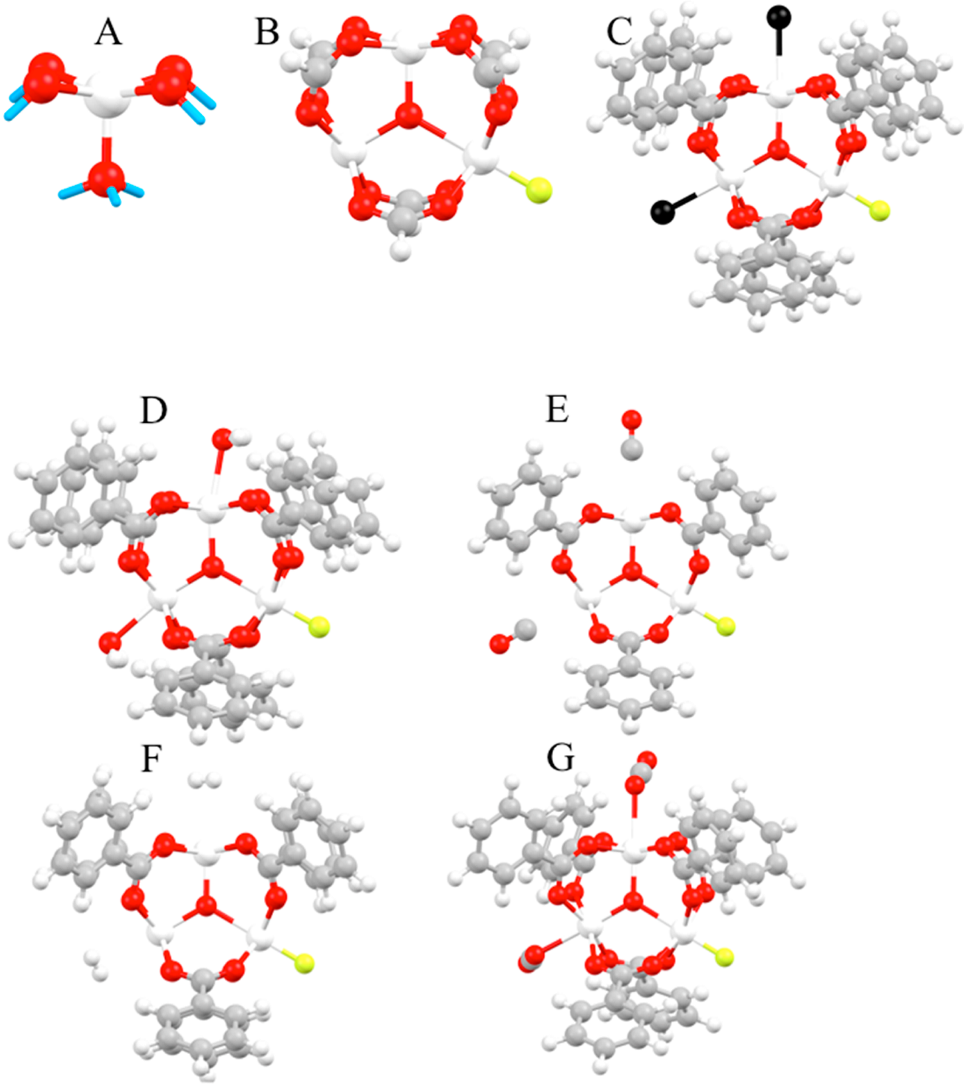

Figure 1. Structures of the (A) **M1**, (B) empty **M3XF6**, and (C) empty **M3XB6** models. Adducts of the **M3XB6** model with the (D) H_2O, (E) CO, (F) H_2, and (G) CO_2 guests. The added protons of the **M1** model are shown in a blue stick model representation. The free axial positions of the metal center are shown in black color. [Color scheme: metal (white), oxygen (red), carbon (gray), hydrogen (light gray), counteranion X (yellow).]

In many recent review articles, the importance of exposed metal sites in gas storage and separation has been emphasized.[9,28−31] However, an important building block, which further involves a cationic species that is expected to exhibit an intriguing interplay with the metal sites, has not yet been studied for its gas adsorption properties. Here, we report how the different metals affect the binding of H_2O, H_2, CO, and CO_2 on the $M^{III}{}_3(\mu_3\text{-O})X(COO)_6$ building unit, which possesses undercoordinated metal sites. X corresponds to the counteranion (typically F^-), which is used to saturate the charge in the trinuclear model complexes. Several variants of this oxo-centered trinuclear cluster with M = Al, Sc, V, Mn, Fe, Cr, Ga, Ru, Rh, In, and Ir analogues have been reported experimentally as isolated species.[32] In some cases, the cluster is composed of mixed-valence metals.

This oxo-centered trinuclear topology has already been used as building block to synthesize several variants of aluminum, scandium, vanadium, chromium, iron, and indium MIL-100, MIL-101, and MIL-127 (also known as socMOF) MOFs.[33−44] Only the Ru, Rh, and Ir analogues have not yet been used in a MOF synthesis. A recent work has shown that the cation in the Cr-MIL-101 MOF can be post-synthetically exchanged by other cations such as Fe and Al.[45] Thus, it is likely that the synthetic procedure of partial post-synthetic exchange of metal cations can also be used in the case of the not-yet-synthesized Ru, Rh, and Ir analogues.

In the present work, a combinatorial computational screening based on DFT is performed for the binding of the H_2O, H_2, CO, and CO_2 molecules with all possible variations of the $M^{III}{}_3(\mu_3\text{-O})X(COO)_6$ trimetallic unit, with M = Al^{3+}, Sc^{3+}, V^{3+}, Cr^{3+}, Fe^{3+}, Ga^{3+}, Rh^{3+}, In^{3+}, Ir^{3+}. The DFT methodology is benchmarked against accurate WFT calculations on smaller models of the trimetallic building block and available experimental data for enthalpies and frequencies. The screening addresses interaction energies, adsorption enthalpies, and vibrational properties. The interactions are analyzed by employing energy decomposition schemes, the electronic density redistribution plots, and natural bonding orbitals (NBOs).

DOI: 10.1021/acs.inorgchem.5b00689
Inorg. Chem. 2015, 54, 8251−8263

■ METHODS

1. Description of the Model Systems. The large size of the unit cell, containing typically more than 400 atoms, suggests to employ finite-size cluster models to approximate the structure of the MOFs. In order to calibrate the accuracy of our methodology, clusters of increasing size have been used. The first, which is denoted as "**M1**", is a monometallic model system. This allows us to move beyond DFT and calculate highly accurate interaction energies by means of post-Hartree–Fock methods (post-HF). The model is composed of one metal atom and its five neighboring O atoms. Four of the O atoms, which belong to the carboxylate groups of the trimetallic molecule, are bound to protons, whereas the fifth O atom, which is centrally coordinated to three metals (μ_3-O), is saturated with three protons. The final cluster is neutral while the metal retains the same coordination environment as in the building block. Several restrictions are applied for the geometry optimization to ensure that the coordination environment is preserved. Only the bonds between the oxygen and the added protons are allowed to relax, whereas the angles and dihedral angles involving these protons and the O atoms are frozen. These restrictions impose that the same coordination environment is kept on the metal atom as in the MOF. To calculate the interactions of the **M1** model with the guest molecules, some restrictions are imposed: (i) the geometry of the **M1** model is kept fixed, and (ii) only the coordinates of the guest are allowed to relax. This structure is presented in Figure 1, as well as in Figure S1 in the Supporting Information.

The second model, which is called "**M3F6**", contains the $[M_3O]^{7+}$ core saturated with six formate $[OOCH]^-$ anions and possesses a total +1*e* charge. This charged building block has been used to evaluate the possible spin states of the unit with spin-polarized atoms by means of single-reference DFT and multireference WFT methods. For all other cases, a F^- counteranion is added as an axial ligand on one of the vacant metal sites and the system is neutralized. The model in this case is denoted as "**M3XF6**". The largest model, which is named as "**M3XB6**", is created by replacing the hydrogen atom of the formate group of the **M3XF6** model by a phenyl ring. Additional calculations are performed to study how the counteranion affects the binding energies and frequencies of the adsorbed molecule on the metal site. This is done for H_2 and CO on the scandium analogue of the M3XF6 model, as an example case only. In a future work, more metal analogues will be included in order to confirm the assumption about the effect of the counteranion.

2. Computational Details. If not mentioned elsewhere, DFT and post-HF calculations have been performed with the TURBOMOLE program package.[46,47] For the **M3F6** and **M3XF6** models, the structures have been optimized under appropriate symmetry restrictions, whereas, for the **M1** models, the structures have been optimized under the geometric constraints described in the previous section. The structures are verified to be minima on the potential energy surface by analytical frequency calculations, using the AOFORCE module.[48] For the **M3XB6** models, no symmetry restrictions were applied during the geometry optimization.

The DFT calculations were performed by using several exchange-correlation functionals in combination with the def2-TZVP or def2-TZVPP basis sets.[49,50] These basis sets account for relativistic effects by using an effective core potential of 28 electrons for In and Rh and of 60 electrons for Ir. To account for weak interactions, the dispersion correction schemes of Grimme (denoted as D2 or D3) were used.[51] For the geometry optimization procedure, the geometries of the structures were optimized with the STATPT module, until the forces were $<10^{-5}$ hartree/bohr and the energy change was $<10^{-7}$ hartree. The convergence criterion for the energy calculation during the self-consistent-field procedure was set to 10^{-8} hartree. For the DFT calculations, the grid m5 was used. Second-order Møller–Plesset (MP2) calculations were carried out with the RICC2 module and the corresponding auxiliary basis sets for the resolution-of-identity (RI) approximation.[52,53] The zero-point energies (ZPEs) and enthalpies were calculated within the harmonic approximation. The choice of DFT method and basis set was based on the best agreement with accurate WFT results and the available experimental data for frequencies and enthalpies of adsorption of H_2, CO, and CO_2 on several MOFs containing the trimetallic moiety. Comparison of these available data with results from other density functionals is discussed in this section and in Tables S1 and S2 in the Supporting Information.

For further validation of the late transition-metal atoms, CCSD(T) values were obtained for Ir and Rh. Here, we used standard Dunning's basis sets,[54,55] together with a l^{-3} extrapolation[56,57] for MP2 and a l^{-5} extrapolation[58] for Hartree–Fock, where l is the angular momentum quantum number of the basis set. For MP2, the complete basis set (CBS) limit is estimated with the basis sets of aug′-cc-pVTZ and aug′-cc-pVQZ quality, where diffuse functions were used on all C, O, and F atoms. To obtain the CCSD(T)/CBS values, we used a subtractive scheme in which we added the difference of MP2 and CCSD(T) to the MP2/CBS values, using a basis set of aug′-cc-pVDZ quality. While these numbers are unlikely to be as accurate as the obtained explicitly correlated (F12) values for the Al- and Sc-containing species, they probably give a solid post-HF estimate of the host–guest interaction energies. In order to save computer time (because the CCSD(T) calculations were rather demanding), we refrained from using a counterpoise correction for these calculations.

Two energy decomposition analysis schemes were carried out on the **M3XF6** models to analyze the interactions of the trimetallic units with the adsorbed molecules. In the first scheme, the binding energy can be written as the sum of the interaction energies (ΔE_{int}) and the deformation energies (ΔE_{def}) of the monomers. ΔE_{int} is further decomposed into terms that contain (i) the electrostatic interactions between the unperturbed charge distributions of the deformed fragment with the field of the other, (ii) the Pauli repulsion, which is associated with going from the unperturbed individual fragments to a symmetrized and orthonormalized wave function of their product $\Psi^0 = NA[\Psi_A\Psi_B]$ that obeys the Pauli exclusion principle (here, N is a normalization constant and A the antisymmetry operator), and (iii) orbital interactions that account for electron pair bonding, charge transfer, and polarization effects when going from Ψ^0 to the converged wave function of the complex.[59] The first two terms can be combined and the sum of the electrostatic interactions and Pauli repulsion is called *steric interaction*. The orbital interactions can be further decomposed by employing the natural orbitals for chemical valence (NOCV) theory, in combination with the extended transition state (ETS) method.[60,61] The ETS-NOCV decomposes the orbital interactions into different components (σ, π) of the chemical bond. These calculations have been performed with the ADF program using similar computational details as previously noted, that is, the PBE0-D3 functional and the TZP basis set.[62] The results obtained with this scheme are denoted as EDA. Because of program limitations, the EDA has been performed only on the **M3XF6** building units with closed-shell spin configuration.

The second energy analysis scheme is the symmetry-adapted perturbation theory (SAPT) employing DFT for the fragment calculations. Concerning such DFT-SAPT calculations,[63,64] the MOLPRO package was utilized.[65] Here, we used the def2-SVP and def2-TZVPP basis sets for the heavy atoms (because of the lack of fitting functions for these atoms), as well as the aug-cc-pVXZ basis sets for C, O, and F, and cc-pVXZ for hydrogen. The dispersion energy was extrapolated with the above-mentioned l^{-3} formula and an asymptotically corrected PBE0 functional was employed for the underlying DFT calculation.[63] The kernel for the DFT-SAPT calculations was the adiabatic local density approximation (ALDA) kernel, whereas by construction, all DFT-SAPT calculations were counterpoise-corrected. The DFT-SAPT energies were partitioned into polarization, exchange, induction, and dispersion terms. For simplicity, the exchange and induction terms are summarized and presented as induction energies. Because of program limitations, only the closed-shell cases were studied.

Multireference (MR) WFT calculations were performed for the chromium **M3F6** models in order to elucidate the total spin of their ground state. The high and low spin states of the empty and loaded clusters were studied, taking into account the adsorbate gases H_2, CO, and H_2O. Orbitals were optimized with the state-average complete-

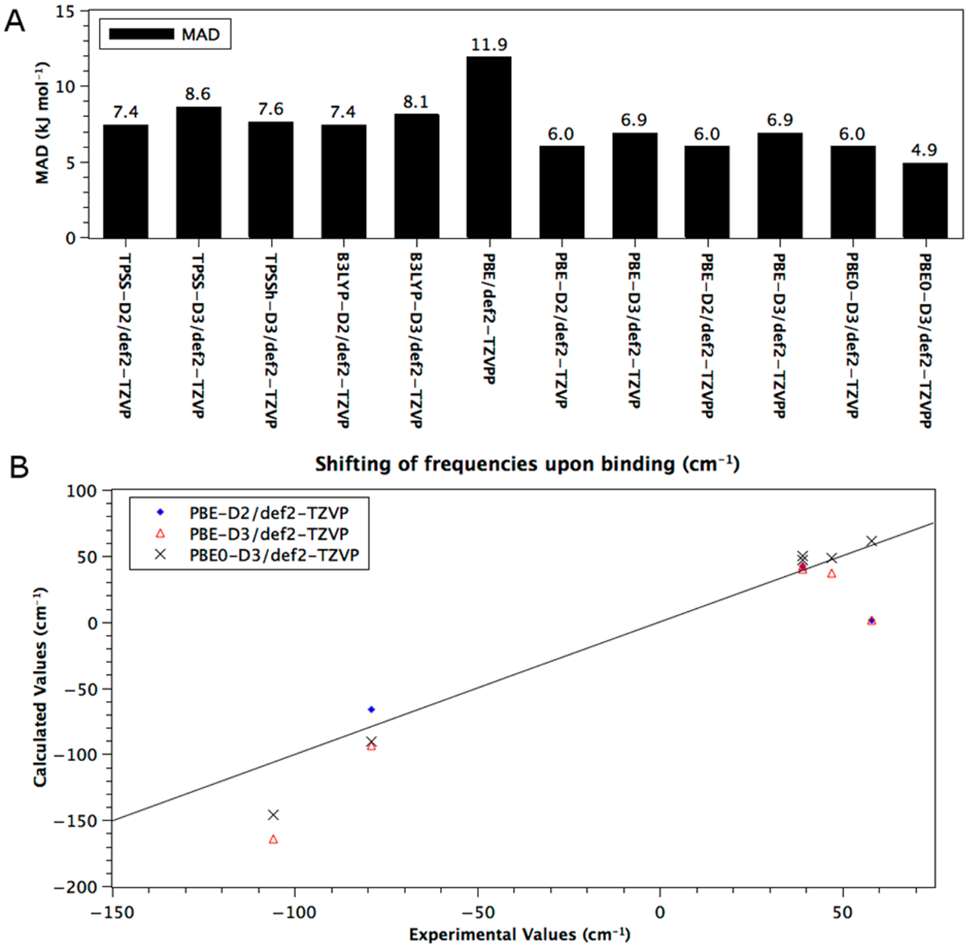

Figure 2. Benchmark of the functionals versus (A) accurate CCSD(T)/CBS results (upper part) and (B) experimental vibrational frequencies (lower part).

active-space self-consistent-field (SA-CASSCF) method and dynamic electron correlation was added from second-order perturbation theory (CASPT2). The active space that was used includes 9 electrons occupying the 9 molecular orbitals composed of the t_{2g} atomic orbitals of the three Cr atoms and is abbreviated as (9,9). The cc-pVTZ basis set of Dunning was chosen for the metal centers, while the cc-pVDZ basis set was used for the remaining atoms.[66,67] In a previous work, it had been shown that this combination of basis sets can reproduce the manifold of different spin states of the oxo-bridged trichromate formates very accurately.[68] The multireference results are compared to broken-symmetry DFT calculations and prove that DFT is able to reproduce the high spin-low spin splitting with reasonable accuracy. Furthermore, it has been examined whether the binding energies, adsorption enthalpies, and vibrational frequencies of the adsorbed molecules are dependent on the ferromagnetic or antiferromagnetic spin state of the **M3F6** model. This is done for the Cr case, and it will be shown that the parallel and antiparallel spin configurations show almost identical results for the interaction energies and frequencies. This allows us to avoid the broken-symmetry DFT approach, where issues such as convergence problems and spin contamination usually appear. Using the high-spin parallel configuration has been a common approach to study the interactions of small molecules with the unsaturated copper centers of the Cu-HKUST-1 MOF.[68,69]

For the treatment of the **M1** model, several restrictions were applied for the geometry optimization to ensure that the coordination environment is preserved. These constraints have been already mentioned in the "Models" section. However, we can compare the accuracy of various density functionals with highly accurate wave function methods. For that reason, the structures were optimized with the MP2/def2-TZVPP method and, as a next step, single-point energy calculations were performed by using several density functionals along with the def2-TZVP basis set and compared with highly accurate WFT results. The reference interaction energies were obtained from the coupled-cluster singles-and-doubles approach with a perturbative correction for connected triple excitations (CCSD(T)). It is well-known that the CCSD(T) method provides acceptable accuracy when very large basis sets are used (at least of quintuple-zeta quality). Alternative CCSD(T) approaches that reduce the computational effort without a loss of accuracy employ explicitly correlated wave functions or extrapolation schemes.[70−72] We have already shown that the addition of terms from interference-corrected explicitly correlated MP2 theory (INT-MP2-F12)[73] to the CCSD(T) energies can yield very accurate atomization[74] and noncovalent interaction[75,76] energies. This method is abbreviated as CCSD(T)+F12+INT and it has been used in the present study for benchmarking the interactions between the H_2 and CO molecules with the **M1** model.

In all DFT and WFT calculations for the latter analysis, the interaction energies are corrected for the basis set superposition error (BSSE) by using the correction scheme of Boys and Bernardi.[77]

3. Calculation of Thermodynamic Properties. The thermodynamic properties are computed for the large **M3XB6** model, by taking the (vibrational) thermal corrections from the smaller **M3XF6** cluster. The binding energies (BE) and adsorption enthalpies (ΔH_{ads}) are calculated as follows:

$$\text{BE} = \frac{E(\text{MOF}\ldots 2\text{gas}) - E(\text{MOF}) - 2E(\text{gas})}{2} \tag{1}$$

$$\Delta H_{\text{ads}} = \frac{H(\text{MOF}\ldots 2\text{gas}) - H(\text{MOF}) - 2H(\text{gas})}{2} \tag{2}$$

where

$$H(\text{MOF}\ldots 2\text{gas}) = E(\text{MOF}\ldots 2\text{gas}) + \text{ZPE}(\text{MOF}\ldots 2\text{gas}) + E_{\text{thermal}}(\text{MOF}\ldots 2\text{gas}) \quad (3)$$

$$H(\text{MOF}) = E(\text{MOF}) + \text{ZPE}(\text{MOF}) + E_{\text{thermal}}(\text{MOF}) \quad (4)$$

$$H(\text{gas}) = E(\text{gas}) + \text{ZPE}(\text{gas}) + E_{\text{thermal}}(\text{gas}) + \frac{7}{2}RT \quad (5)$$

$$\text{ZPE} = \sum_i \frac{h\nu_i}{2} \quad (6)$$

$$E_{\text{thermal}} = \sum_i \frac{h\nu_i}{\exp\left(\frac{h\nu_i}{kT}\right) - 1} \quad (7)$$

The (7/2)RT term is added to H(gas) to account for (i) the rotational contributions (equal to (2/2)RT, because H_2, CO, and CO_2 are linear), (ii) the translational degrees of freedom ((3/2)RT), and (iii) the PV factor (ideal gas behavior is assumed, so PV equals RT for 1 mol of gas).

■ RESULTS

1. Functional and Basis Set Study. The choice of density functional and basis set that can provide accurate interaction energies and vibrational properties is discussed in this section. A set of accurate CCSD(T)/CBS results and experimental frequencies are used as reference data. In the upper part of Figure 2, the mean absolute deviation (MAD) is shown for combinations of several functionals with the def2-TZVP or def2-TZVPP basis sets. Among all combinations studied, the PBE0-D3/def2-TZVPP has the smallest MAD (4.9 kJ mol^{-1}), followed by the PBE-D2, PBE-D3, and PBE0-D3 functionals combined with the def2-TZVP basis set (6.0, 6.9, and 6.0 kJ mol^{-1}, respectively). Because of the higher computational cost of the def2-TZVPP basis set compared to the smaller def2-TZVP set, the use of the smaller basis set is desirable. We chose to further evaluate the performance of these three functionals against the available experimental vibrational frequencies of H_2 and CO adsorbed on the Al, Sc, Cr, and Fe building blocks. The shift of the vibrational frequencies of the guest molecules upon binding is considered, rather than their absolute frequencies. The calculated shifts are plotted against the experimental values in the lower part of Figure 2. Results suggest that PBE-D3 performs well for Al and Sc, but provides poorer results for Cr and Fe. On the other hand, PBE0 shows an overall better agreement for all metals and both H_2 and CO. Since we were interested in a method that can provide reliable interaction energies as well as vibrational frequencies, the PBE0-D3/def2-TZVP level of theory was chosen for our final study.

2. Bare and Hydrated Building Blocks. As a first step, the geometry and spin state of the bare and hydrated **M3F6** models were calculated with DFT. The geometries of the model systems were optimized by assuming the high-spin ferromagnetically coupled spin configuration for V, Cr, and Fe. In all other cases, the metal atoms have closed-shell spin configurations. The results show that the ground spin state of V^{III} has 2 unpaired electrons per metal atom, whereas that of Cr^{III} has 3 and that of Fe^{III} has 5. Consequently, all M3X6 and M3XF6 models are considered to be in the ferromagnetic spin state. Thus, the ground spin state has 6 unpaired electrons for the vanadium, 9 for the chromium, and 15 for the iron trimetallic building blocks.

As a next step, the geometries of the M3XF6 and M3XB6 models were optimized in the presence of the F^- counteranion, which imposes a symmetry reduction as the M-(μ_3)O bonds are no longer equivalent. The metal atom, which is coordinated to the F^- anion, has longer M-(μ_3)O bonds than the other undercoordinated metal atoms. The results are summarized in Table 1.

Table 1. Spin Multiplicity (2S+1) and Main Geometric Parameters for the Empty and Hydrated M3XB6 Model[a]

	Empty		Hydrated		
	2S +1	M–$O_{central}$[b] (pm)	M–$O_{central}$[b] (pm)	M–O_{water} (pm)	binding energy, BE (kJ mol^{-1})
Al	1	174 [187]	179 [192]	209	−64.1
Sc	1	190 [223]	193 [221]	234	−74.9
V	7	183 [205]	186 [206]	219	−80.8
Cr	10	183 [200]	186 [199]	216	−83.5
Fe	16	184 [207]	186 [209]	225	−64.4
Ga	1	181 [188]	184 [191]	213	−65.4
Rh	1	189 [198]	191 [198]	217	−89.3
In	1	199 [202]	201 [205]	229	−77.3
Ir	1	193 [199]	195 [200]	217	−97.8

[a] H_2O binding energies are also reported. [b] Distances in brackets refer to the metal atom that is coordinated to the F^- counteranion.

The undercoordinated M_3O complexes yield relatively strong interactions with H_2O. The binding energies range from −64 to −100 kJ mol^{-1}, with the highest values calculated for Rh and Ir. The distances between the metal and the central oxygen are elongated by ~3 pm upon H_2O binding. In all cases except for Sc and Cr, the metal coordinated to the F^- counteranion shows a metal−oxygen distance elongated by ~3 pm.

3. Interaction with CO. Carbon monoxide adsorbed on MOFs with exposed metal sites is widely studied, because it can give important information about the coordination number as well as the oxidation and spin state of the metallic centers of the MOFs. CO is bound in a linear way through the C atom. Results from the present work and from previous experimental studies are summarized in Table 2. In all cases, the metal retains the same spin state upon coordination with CO and no spin transition occurs as in the case of M-CPO-27 with CO.[23] For the case of Fe, the other two possible spin states with 3 and 1 unpaired electrons per iron atom were calculated. They were ~250 kJ mol^{-1} higher than the ground spin state with 5 unpaired electrons per Fe.

The calculated values for enthalpy and frequencies are in very good agreement with the available experimental results. In some experiments, a hydroxide is used as counteranion. As is shown in Table S8 of the Supporting Information, the counteranion has a negligible effect on the binding energies and frequencies of the CO adsorbed on the scandium analogue, so the values calculated for the $M_3O(F)$ building unit may be compared with the one of $M_3O(F_x,OH_{1-x})$ stoichiometry. For most metals, the enthalpies of adsorption are in the range from −25 kJ mol^{-1} to −30 kJ mol^{-1}. For V and Cr, the values are ca. −40 and −47 kJ mol^{-1}, respectively. Yu et al. have calculated a value of −37 kJ mol^{-1} for the Cr analogue.[78] For these metals, interactions are weaker compared to those with water by ~30 kJ mol^{-1}. These values are within the same range for the various analogues of M-CPO-27, with M(II) = Mg, Mn, Fe, Co, Ni, and Zn. DFT enthalpies from −25 kJ mol^{-1} to −40 kJ mol^{-1} are reported, with Zn having the lowest enthalpy and Ni the

DOI: 10.1021/acs.inorgchem.5b00689
Inorg. Chem. 2015, 54, 8251−8263

Table 2. Energetic, Vibrational, and Main Geometric Parameters for the Adsorption of CO on the M3XB6 Model[a]

	binding energy, BE (kJ mol^{-1})	ΔH (kJ mol^{-1}) 0 K	ΔH (kJ mol^{-1}) RT	$\Delta\nu$ (cm^{-1})	R[M–CO] (pm)	R[M–O$_{central}$][b] (pm)
Al	−28.1	−25.3	−25.7	+49 (+41 to + 52)[c]	239	177 [190]
Sc	−34.3	−31.8	−31.4	+52 (+39)[d]	264	192 [222]
V	−42.8	−40.2	−40.7	+48	235	186 [205]
Cr	−49.5	−46.5	−47.5	+61 (+54,+57,+64)[e]	228	186 [200]
Fe	−29.7	−28.5	−28.3 (−28 to −39)[f]	+48 (+47)[f]	249	185 [208]
Ga	−29.1	−26.6	−26.6	+52	243	183 [190]
Rh	−122.7	−117.4	−119.6	−18	192	193 [198]
In	−39.1	−35.9	−35.8	+66	253	200 [204]
Ir	−202.8	−195.0	−197.7	−68	188	198 [203]

[a] Interaction energies and adsorption enthalpies are given per CO molecule. Distances refer to the carbon atom of the CO molecule. [b] Distances shown in brackets refer to the metal atom that is coordinated to the F$^-$ counteranion. [c] Al(OH)-MIL-100 from ref 94. Our calculated value for $Al_3O(OH)$ is +45 cm^{-1}. Value given in parentheses corresponds to the experimental value. [d] Sc(OH)-MIL-100, from ref 83. The calculated value for $Sc_3O(OH)$ is +48 cm^{-1}. Values given in parentheses correspond to the experimental values. [e] Cr-(F_xOH_{1-x})-MIL-100, from ref 15. The calculated value for $Cr_3O(OH)$ is +55 cm^{-1}. Values given in parentheses correspond to the experimental values. [f] Fe-(F_xOH_{1-x})-MIL-100, from ref 92. Values given in parentheses correspond to the experimental values.

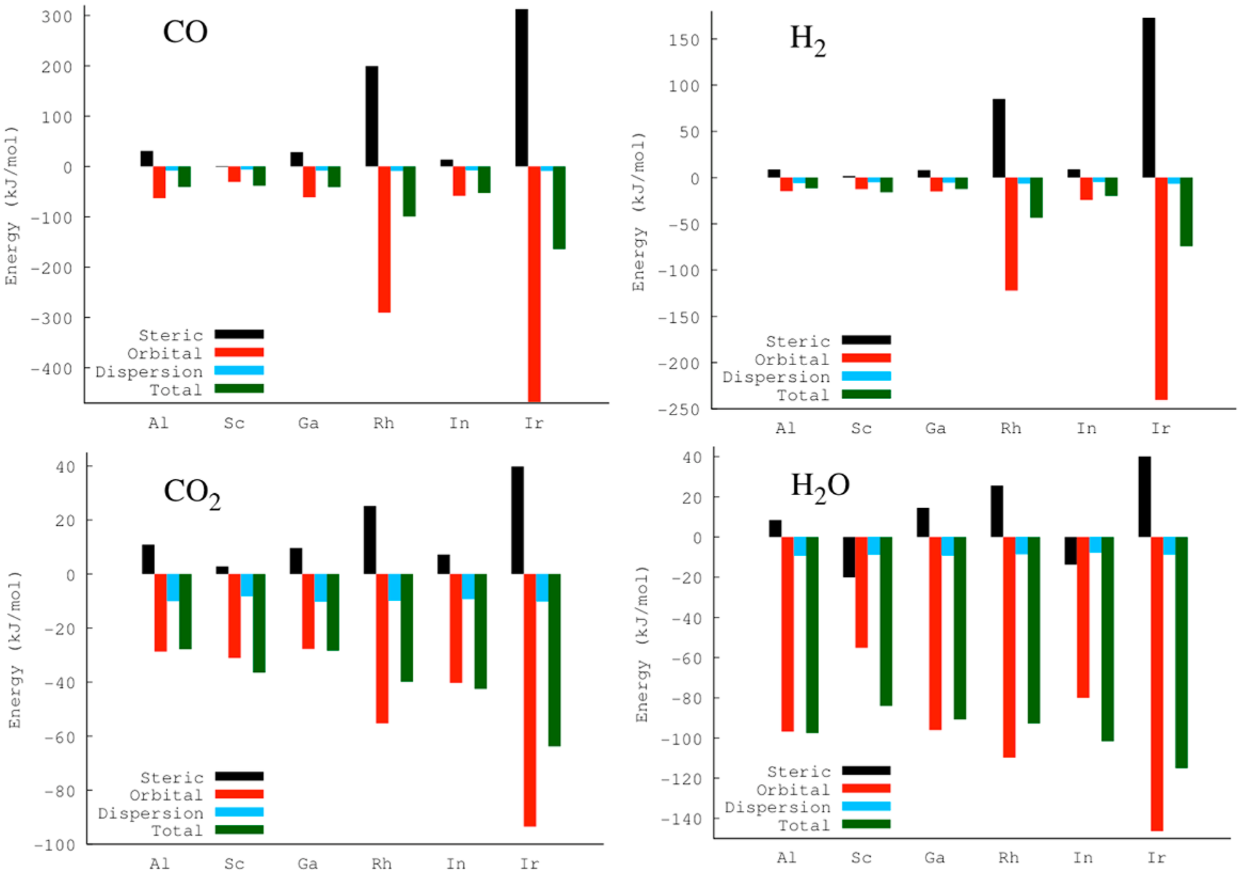

Figure 3. Graphical representation of the energy decomposition analysis (EDA) into steric (black), orbital (red), dispersion (cyan), and total bonding (green). Energy units are given in kJ mol^{-1}.

highest enthalpy.[79] CO shows almost the same binding enthalpies of −30 kJ mol^{-1} with both Fe^{II} and Fe^{III} sites of Fe^{II}-CPO-27 and Fe^{III}$_3$O(F), respectively. Notable exceptions are found for the noble metals Rh and Ir, which show large binding energies of approximately −120 kJ mol^{-1} and −200 kJ mol^{-1}, respectively. Similar values for the interaction energies are also obtained with the CCSD(T) approach, −135 and −172 kJ mol^{-1}, respectively, thus indicating that the PBE0-D3 energies are reliable but there is no obvious trend concerning the question whether PBE0-D3 is overestimating or underestimating the CCSD(T) values. One possible explanation is that the CCSD(T) calculations have been performed on PBE0-D3 geometries and the equilibrium bond lengths could be quite different from those obtained after optimization at the CCSD(T) level. This is beyond the scope of the present work and could be the topic of a separate study. CO adsorption to Rh and Ir is stronger than the absorption to water, by 30 and 100 kJ mol^{-1}, respectively, while the corresponding CCSD(T) values are 25 and 60 kJ mol^{-1}.

Table 3. Energetic, Vibrational, and Main Geometric Parameters for the Adsorption of H_2 on the M3XB6 Model[a]

	binding energy, BE ($kJ\ mol^{-1}$)	ΔH ($kJ\ mol^{-1}$) 0 K	ΔH ($kJ\ mol^{-1}$) RT	$\Delta \nu$ (cm^{-1})[b]	ΔR(H−H)[b] (pm)	R[M−com H_2] (pm)	R[$M-O_{central}$] (pm)
Al	−9.7	−2.5	−4.6	−81	0.33	258	174
Sc	−14.0	−7.2	−8.7 (−6.9, −11.2)[c,d]	−92 (−79)[d]	0.47	260	191
V	−16.7	−7.2	−10.1	−128	0.70	232	184
Cr	−18.0	−7.6	−10.6 (−6.9, −9.5)[e]	−146 (−111, −101)[e]	0.82	220	184
Fe	−12.5	−6.5	−8.0	−116	0.41	263	184
Ga	−9.4	−1.7	−3.8 (−6.7)[f]	−94	0.38	259	181
Rh	−42.1	−26.1	−31.3	−559	4.02	180	191
In	−13.7	−5.5	−7.9 (−6.7 to −6.4)[f,g]	−125	0.67	250	199
Ir	−82.2	−63.2	−69.3	−1236	10.28	168	195

[a] Interaction energies and adsorption enthalpies are expressed per H_2 molecule. [b] The frequency of free H_2 is calculated to 4421 cm^{-1} and the bond length to 74.61 pm. [c] $Sc_3O(OH)$ $(BTB)_2$, from ref 82. Value in parentheses corresponds to the experimental value. [d] $Sc_3O(OH)$-MIL-100, from ref 83. Value in parentheses corresponds to the experimental value. [e] Values refer to Cr(F_xOH_{1-x})-MIL-100 and Cr(F)-MIL-101, respectively, from ref 84. Values in parentheses correspond to the experimental values. [f] Values refer to In-(NO3)-MIL-127 and Ga-(NO3)-MIL-127 from ref 44. Value in parentheses corresponds to the experimental value. [g] In(NO_3)-socMOF, from ref 87. Values in parentheses correspond to experimental values.

The vibrational frequency of adsorbed CO is blue-shifted by 50−60 cm^{-1}, with respect to the free molecule. Comparable values have also been calculated for M-CPO-27.[79] The only exceptions for the trimetallic building blocks are found again for the Rh and Ir noble metals. The C−O frequencies are red-shifted by 20 and 70 cm^{-1}. Similarly, we find that the Rh−CO and Ir−CO distances of ~190 pm are significantly smaller than the other M−CO distances, which are in the range of 230−250 pm. A similar trend is observed for the C−O bond length. The C−O bond gets elongated by 2 pm, when it interacts with Rh and Ir, whereas it does not change in the other cases.

These results indicate that the interactions of the metals with carbon monoxide are different in nature for these cases. The red-shift hints at significant π back-donation from the occupied metal orbitals to the π^* antibonding orbitals of CO. To underpin this, we used the method of Weinhold to calculate natural bond orbitals (NBO) and charges based on the natural population analysis (NPA),[80] as implemented in the Gaussian09 package.[81] In all cases, there is a charge transfer of 0.2−0.3 e from the carbon monoxide molecule to **M3XF6**. The analysis of the NBOs showed that, in the case of Rh- and Ir-**M3XF6**, there was a significant charge occupation on the π^* antibonding orbitals of CO. According to the calculations, back-donation from the Rh and Ir atoms is estimated to be 0.15 e and 0.25 e, respectively, while it is zero for all other cases.

This behavior is also verified by the energy decomposition analysis, which is presented graphically in Figure 3 and in more detail in Table S9 of the Supporting Information. For Rh and Ir, very large negative values of −290 and −470 kJ mol^{-1} for the orbital interactions are calculated, whereas the steric interactions get very positive values of +200 and +310 kJ mol^{-1}, respectively, which destabilize the complex. For all other metal cases, the steric interactions have small positive values with a maximum of 30 kJ mol^{-1} and moderate values for the orbital interactions between −30 and −60 kJ mol^{-1}. Dispersion interactions are small for all cases (<10 kJ mol^{-1}).

4. Interaction with H_2. Dihydrogen is bound in a side-on way, resulting in a T-shaped η^2-configuration with the metal center. The important structural, vibrational, and thermodynamic parameters are summarized in Table 3. The binding energies vary between −10 kJ mol^{-1} and −20 kJ mol^{-1}. Only exceptions were found for the Rh and Ir complexes, where much higher values of −42 and −82 kJ mol^{-1}, respectively, were obtained. Similarly to the CO interaction energies, the PBE0-D3 energies for Rh and Ir underestimate the reference CCSD(T) values (−54 and −100 kJ mol^{-1}, respectively).

The calculated values are in good agreement with available experimental enthalpies. The computed enthalpy of approximately −9 kJ mol^{-1} for Sc falls in the range of the two experimental values of −7 and −11 kJ mol^{-1}.[82,83] Good agreement is also observed for the frequency shift of adsorbed H_2, which is calculated to be −79 cm^{-1}, whereas the experimental value is −92 cm^{-1}. The values for Cr are overestimated, with respect to experiment. The adsorption enthalpy is estimated at approximately −10.5 kJ mol^{-1}, which is slightly larger than the reported values of −9.5 and −6.9 kJ mol^{-1} for Cr(F_xOH_{1-x})-MIL-100 and Cr(F)-MIL-101, respectively.[84] The calculated H_2 stretching frequency is also overestimated by ~40 cm^{-1}, with respect to the reported experimental values of −111 and −101 cm^{-1}. The binding enthalpies and stretching frequencies for the early metals have similar values with the M-CPO-27 series, which exhibit enthalpy values between −10 and −15 kJ mol^{-1}.[85] The stretching frequencies are shifted from −70 cm^{-1} to −130 cm^{-1}. Comparable values were also reported by Woo et al. for various metal-substituted porphyrin systems intercalated in planar graphene.[86] In that work, the highest interaction energies were reported for Ti (−33 kJ mol^{-1}) and V (−22 kJ mol^{-1}), followed by Ca, Mg, and Zn, with values of approximately −10 kJ mol^{-1}. The adsorption enthalpies for Ga and In follow different trends. The computed value for Ga is lower than that observed in the experiment (−3.8 kJ mol^{-1} versus −6.7 kJ mol^{-1}),[44] but is higher for In, by 1−1.5 kJ mol^{-1} (−7.9 kJ mol^{-1}, versus −6.7 and −6.4 kJ mol^{-1}).[87] For these two cases, experiments have been conducted on the MIL-127 analogue, which contains $[NO_3]^-$ as the counteranion.

Similar to the CO case, higher enthalpies of approximately −31 and −70 kJ mol^{-1} are calculated for Rh and Ir, respectively. The H_2 molecule is significantly elongated by 4 and 10 pm, respectively, when it interacts with these two metal centers. This remarkable distortion is also reflected in the stretching frequency, which is red-shifted by 560 and 1230 cm^{-1}, respectively. The distance between the dihydrogen center of mass and the two noble metals is much shorter, compared to the other cases. The optimized distances are 180 and 168 pm but ~250 pm for all other cases. The dimer can be considered

Table 4. Energetic and Main Structural Parameters for the Adsorption of CO_2 on the M3XB6 Model[a]

	binding energy, BE (kJ mol^{-1})	ΔH (kJ mol^{-1})		$R(M\cdots O_{OCO})$ (pm)	$\theta[M-O-C_{OCO})]$ (deg)	$\theta[O-C-O]$ (deg)
		0 K	RT			
Al	−25.5	−25.1	−23.7	260	112.9	178.7
Sc	−35.4	−34.9	−34.6	250	117.3	178.2
V	−33.6	−33.4	−33.6	242	117.3	178.4
Cr[b,c,d]	−35.8	−36.1	−35.0 (−62,[b] −44,[c] −25[d])	236	116.2	178.3
Fe[e]	−27.7	−28.1	−26.7 (−25 to −35)	255	113.6	178.5
Ga	−26.0	−25.4	−23.9	260	113.2	178.5
Rh	−37.8	−37.5	−36.1	234	115.8	178.3
In[f]	−33.5	−32.4	−31.1 (−28.5)	254	116.6	178.1
Ir	−42.8	−41.7	−40.7	230	117.8	178.1

[a] Interaction energies and adsorption enthalpies are given per CO_2 molecule. [b] Cr(F)-MIL-100/101, values of −62 and −44 kJ mol^{-1}, from ref 89. [c] Cr(F)-MIL-101, value of −44 kJ mol^{-1} from ref 90. Values in parentheses correspond to the experimental values. [d] Cr(F)-MIL-101, value of −25 kJ mol^{-1} from ref 91. Values in parentheses correspond to the experimental values. [e] $Fe(F_xOH_{1-x})$-MIL-100, from ref 92. Values in parentheses correspond to the experimental values. [f] $In(NO_3)$-socMOF, from ref 87. Values in parentheses correspond to the experimental values.

as an η^2-complex, where H_2 donates electron density to the empty *d*-orbitals of Rh and Ir. The natural population analysis (NPA) shows that there is a charge transfer of 0.15*e* and 0.25*e* from H_2 to Rh and Ir, respectively. For all other cases, the charge transfer is almost negligible, with Cr having the next largest charge increase of 0.1*e*. Similar conclusions are drawn from the EDA scheme. Very large negative contributions of −120 and −240 kJ mol^{-1} for Rh and Ir are estimated for the orbital interactions with significantly smaller values (between −12 and −14 kJ mol^{-1}) for the remaining cases. Steric interactions are quite large for Rh and Ir (+85 and +173 kJ mol^{-1}), whereas, for the other metals, they account to approximately +10 kJ mol^{-1}.

This type of interaction with Rh and Ir is referred to as Kubas-type binding, named after Kubas, who was the first to observe and characterize these weak nondissociative metal−H_2 adducts.[88] For the remaining cases, the adsorption is governed by weak dispersion and charge or dipole-induced dipole interactions. Here, metal atoms are creating an electric field, which polarizes the electronic density of H_2. The nature of this interaction can be illustrated by the electronic density redistribution plots shown in the Supporting Information. This plot is defined as follows: $\Delta\rho = \rho(\text{adsorbent}\cdots H_2) - \rho(\text{adsorbent}) - \rho(H_2)$. The density ρ of each monomer is evaluated at the complex geometry. Excess electronic density is calculated in the area between the metal center and dihydrogen.

Finally, it should be mentioned that the H_2 enthalpy of adsorption (RT or 298 K) on the Rh trinuclear complex (−31.3 kJ mol^{-1}) reaches the target set by the U.S. Department of Energy (approximately −25 kJ mol^{-1}) for viable hydrogen storage. However, the gravimetric capacity is expected to be far below the desired target, because of the low concentration of the active metal sites in the framework. Since the concentration of open metal sites per unit cell in a hypothetical Rh-based MOF is low, the initial high adsorption enthalpy at small H_2 loadings will drop significantly at values of ~10 kJ mol^{-1}. This value corresponds to physisorption on the organic linkers, which will be the only available binding sites after all open metal sites have become saturated with H_2.

5. Interaction with CO_2. Carbon dioxide is bound through a tilted end-on η^1(O) configuration to the metal atom. The angle between the metal atom and the O−C(O) atoms is between 113° and 118°, as summarized in Table 4. The molecule is slightly distorted by ca. 1.5° from its linear conformation. The metal−oxygen distance is 250−260 pm for Al, Sc, Fe, and Ga, and 230−240 pm for V, Cr, Rh, and Ir. The intramolecular $M-O_{central}$ distances in the **M3XB6** model are almost not affected, with respect to the empty building block. The elongation is, at most, 1 pm. The binding energies are in the range between −26 and −43 kJ mol^{-1} (Table 4). The calculated enthalpy for Cr of −35 kJ mol^{-1} is in good agreement with the reported experimental values of −44 and −25 kJ mol^{-1} for Cr(F)-MIL-101, but is lower than the value of −60 kJ mol^{-1} in Cr(F)-MIL-100.[89−91] Comparison of the DFT value for Cr with our most accurate WFT calculations shows that DFT underestimates the interactions with CO_2. A similar value of −30 kJ mol^{-1} has been calculated with the ωB97X-D and B3LYP-D functionals.[78] The PBE0-D3 value of −34.5 is smaller, compared to the best CCSD(T) estimate of −49.1 kJ mol^{-1}. The same trend is also observed for the Rh and Ir cases. The PBE0-D3 values for Rh and Ir are underestimated by ~18 and ~7 kJ mol^{-1}, with respect to the CCSD(T) values of −54.2 and −50.2 kJ mol^{-1}.

For $Fe(F_xOH_{1-x})$-MIL-100, the calculated value of −27 kJ mol^{-1} falls within the measured range of −25 kJ mol^{-1} to −35 kJ mol^{-1}.[92] Similarly, for $In(NO_3)$-socMOF, our computed value of −31 kJ mol^{-1} is in very good agreement with the experimental value of −28.5 kJ mol^{-1}.[87]

In contrast to the H_2 and CO adsorptions on the trinuclear complexes, the CO_2 binding energies[21] are not varying significantly with the choice of the metal. The CO_2 interactions with Rh and Ir are in the same range as with the other metals examined in this work and are not affected significantly by changing the metal cation. However, for M-CPO-27, DFT calculations reveal that some metals have increased interaction energies with CO_2.[20,26]

The charge transfer from CO_2 to the **M3XF6** unit is almost negligible and the maximum value is ca. 0.1 *e* for Sc, V, Cr, Rh, In, and Ir. Polarization of the electron density is observed for CO_2, where the proximal oxygen to the metal atom gains electron density, with respect to isolated CO_2. Similarly, the distant oxygen atom loses electron density. Contributions from dispersion are the same for all systems and reach 10 kJ mol^{-1}. The biggest contribution to the binding comes from the orbital interactions, which are strongest for Rh and Ir, whereas the steric interactions have a tendency to destabilize the complex.

We also tried to analyze the electrostatic effects by considering interactions between a CO_2 molecule and a point charge, as was shown by Park et al.[21] The energy of a CO_2 molecule is calculated in the presence and absence of a point

Table 5. Decomposition of Orbital Interactions (ΔE_{OI}) from the ETS-NOCVs Analysis[a]

		Al	Sc	Ga	Rh	In	Ir
CO	$\Delta V_{electrostatic}$ (kJ mol^{-1})	−99.6 (58%)	−59.4 (60%)	−100.4 (59%)	−453.2 (60%)	−96.6 (59%)	−669.4 (58%)
	ΔE_{OI} (kJ mol^{-1})	−63.2 (37%)	−31.2 (32%)	−61.3 (36%)	−289.9 (38%)	−58.1 (36%)	−467.9 (41%)
	forward-donation (σ CO → M)	−47.1 [0.24]	−22.8 [0.18]	−47.2 [0.26]	−164.8[b] [0.60]	−41.9 [0.25]	−211.3[b] [0.68]
	back-donation (M → π^* CO)	−8.6 [0.20]	−4.4 [0.11]	−6.6 [0.16]	−98.5 [0.69]	−5.5 [0.13]	−164.1 [0.87]
H_2	$\Delta V_{electrostatic}$ (kJ mol^{-1})	−20.9 (51%)	−16.3 (49%)	−21.7 (52%)	−171.2 (57%)	−27.0 (48%)	−340.9 (58%)
	ΔE_{OI} (kJ mol^{-1})	−14.6 (35%)	−12.6 (48%)	−15.0 (36%)	−122.2 (41%)	−24.3 (43%)	−240.3 (41%)
	forward-donation (σ H_2 → M)	−10.9	−10.4	−11.7 [0.13]	−83.0 [0.40]	−18.1 [0.16]	−164.8 [0.50]
	back-donation (M → σ^* H_2)	0.0	0.0	0.0	−20.5 [0.29]	0.0	−50.7 [0.18]
CO_2	$\Delta V_{electrostatic}$ (kJ mol^{-1})	−50.0 (56%)	−55.1 (57%)	−49.0 (56%)	−85.0 (57%)	−62.0 (55%)	−110.8 (51%)
	ΔE_{OI} (kJ mol^{-1})	−28.7 (32%)	−31.3 (32%)	−27.9 (32%)	−54.2 (36%)	−40.0 (36%)	−93.5 (43%)
	forward-donation (π_g CO_2 → M)	−18.7 [0.15]	−19.5 [0.16]	−18.3 [0.16]	−35.6 [0.26]	−24.4 [0.18]	−45.1 [0.29]

[a] Values in brackets correspond to a Löwdin population analysis of the individual bonding term. Values in parentheses show the percentage that electrostatic and orbital interactions contribute to the total attractive interactions ($\Delta V_{electrostatic} + \Delta E_{OI}$). [b] There are also additional interactions that contribute to σ forward-donation.

charge. The molecule and the point charge are taken from the optimized geometry of the **M3XF6−CO_2** model. The partial charge of the metal atom is calculated from a Bader charge analysis.[93] The results are presented in Table S11. Although this simple analysis works for the M-CPO-27,[21] it fails for the trimetallic building blocks and cannot reproduce the correct trend of interaction energies for the different metals. As shown in Table S11, the electrostatic value for Ir is half that for Al, in comparison, whereas the DFT binding energies show opposite behavior. The DFT value for Ir is almost doubled, compared to that for the Al. This suggests that interactions cannot be described by this simple model of a positive point charge.

6. Discussion and Analysis. In this section, we discuss the most important terms that contribute to the binding of CO, H_2, and CO_2. The results from the ETS-NOCV analysis are presented in Table 5. Values in brackets correspond to Löwdin populations of the individual bonding term. Contours for the most important NOCVs are shown in the Supporting Information. For CO, the largest contribution to attractive interactions is from electrostatics. It amounts to ~60% of the total attractive interaction for all metals. As total attractive interaction, we consider the sum of electrostatics, orbital interactions, and dispersion. The orbital interactions can be further separated into forward- and back-donation terms. The largest contribution is due to σ-type bonding with CO. For Al, Sc, Ga, and In, σ-type bonding is ~85% of the total orbital interactions. In accordance to the NBO analysis, a very small contribution from back-donation is calculated for these metals. For the Rh and Ir case, back-donation from the occupied *d* metal orbitals to the π^* antibonding orbitals of CO becomes important and contributes ~40% to the orbital interactions. The NOCVs scheme estimates a significant charge back-donation of 0.7*e* to the π^* antibonding orbitals of CO.

For the cases with partially filled *d* shells, a complementary analysis is done based on the CASSCF orbitals, in order to explain the trends in the binding energies of V, Cr, and Fe with CO. The NPA analysis shows that the charge donation from CO to the metal follows the order V ≈ Cr > Fe. According to the analysis, all metals have a partial charge of 0.2*e* transferred to their empty *p* orbitals, but the main difference is in the *d* orbitals. In Figure 4, a qualitative picture of the splitting of the *d*-orbitals is shown based on the CASSCF results for the M3F6 models. When CO binds, a σ-type coordination bond is formed with the metal center, which changes its local coordination environment from square pyramidal to quasi-octahedral. The change of the crystal field splitting upon CO binding is shown schematically in Figure 4, where the *d*-orbitals of the metal are split into three degenerate t_{2g} orbitals and two e_g. The Fe center, which has a $3d^5$ configuration, cannot accept a donation of electron density from CO to the *d*-orbitals, because they are fully occupied. In contrast, the V and Cr centers have empty e_g orbitals and, thus, electron density from CO can be donated to these orbitals. The NPA analysis shows a partial charge transfer of 0.1*e* to the empty 3*d* orbitals of V and Cr and no charge transfer to the Fe 3*d* orbitals. This lack of charge transfer to the 3*d* orbitals may explain why Fe has the weakest affinity to CO, compared to V and Cr. The NBO analysis did not reveal any significant occupation (<1%) of the π^* antibonding molecular orbitals of CO in the three cases, so no charge back-donation is expected for V, Cr, and Fe.

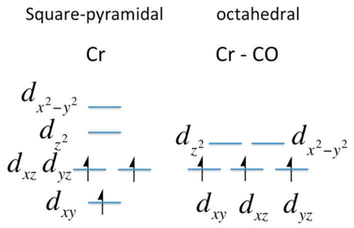

Figure 4. Change of the crystal field splitting from square planar to octahedral field. This qualitatively resembles the situation for the Cr case (d^3) upon CO adsorption.

Similar trends are calculated for H_2. The electrostatic interactions are 60% of the total attractive interactions in all cases, with orbital interactions contributing 40%. Orbital interactions can be further classified into forward- and back-donation terms. For Al, Sc, Ga, and In, the ETS-NOCV scheme calculates only forward-donation from the σ molecular orbital of H_2 to the metal unoccupied orbitals. For Rh and Ir, the back-donation terms become significant and contribute ~20% to the total orbital interactions. The Löwdin population analysis predicts that charges of 0.2*e* and 0.3*e* charge are transferred from the occupied *d*-orbitals from Rh and Ir, respectively, to the σ^* antibonding molecular orbital of H_2.

For CO_2, the highest contribution comes from electrostatic effects. Their average value is 57%, with Ir being an exception with slightly lower contributions (51%). Orbital interactions are estimated at ~34%, with Ir being an exception with higher contributions (43%). Dispersion is estimated between 9% and 11%, with Rh and Ir being exceptions with lower contributions of 7% and 5%. For all metals, a σ-type bonding from the nonbonding π_g molecular orbitals of CO_2 to the unoccupied metal orbitals is calculated but no back-donation to the π^* antibonding orbitals of CO_2. The charge donation is ca. 0.15e for Al, Sc, Ga, and In, and higher (~0.3e) for Rh and Ir. This difference is also depicted in the bonding terms, which are between −18 and −24 kJ mol^{-1} for Al, Sc, Ga, and In but larger in value (−36 and −45 kJ mol^{-1}) for Rh and Ir.

■ CONCLUSIONS

In the present work, a systematic study on the interactions of H_2, CO, and CO_2 with the unsaturated metal centers of the $M^{III}{}_3(\mu_3\text{-O})X(COO)_6$ building blocks (M = Al, Sc, V, Cr, Fe, Ga, Rh, In, Ir) is presented. These building blocks are molecular units of various MOFs, such as MIL-100, MIL-101, and MIL-127. To the best of our knowledge, this is the first in-depth analysis of the noncovalent interactions of this family of trinuclear species with small molecules. The isostructural nature of these molecular species allowed to elucidate the correlation between the electronic structure of the metal center and the binding strength of H_2, CO, and CO_2. For the sake of completeness, the interaction of H_2O with the under-coordinated metal sites was computed and compared with the other guest molecule binding energies.

The choice of the PBE0-D3/def2-TZVP method was calibrated against various accurate wave function calculations and available experimental data. The computational efficiency of DFT allowed us to perform a computational screening on several possible metal variants of this family of building blocks. The strongest interactions were calculated for H_2O, followed by CO ≈ CO_2, and are weakest for H_2. However, the binding strength changes for the Rh and Ir noble metals, with the CO binding being significantly stronger than that for H_2O, because of strong orbital interactions and significant charge back-donation. By means of the ETS-NOCV method, we were able to qualitatively interpret the interactions and explain why Rh and Ir can bind strongly to the guest molecules.

The H_2 binding affinities are moderate and almost none of them are in the desired range for room-temperature (RT) application in hydrogen storage tanks. Only exceptions are the Rh and Ir analogues, which show the highest adsorption enthalpies of −30 and −70 kJ mol^{-1}, respectively, and can form Kubas-type complexes with H_2. Al and Ga centers show very weak binding (between −4 kJ mol^{-1} and −5 kJ mol^{-1}). Sc, V, Cr, and In show intermediate binding (between −9 kJ mol^{-1} and −12 kJ mol^{-1}). The binding of H_2 is mainly due to dispersion and electrostatic interactions. The open metal site is creating a field that induces a dipole moment on H_2. This interaction is visualized by density redistribution plots. Only for the Rh and Ir cases, the results show that there is significant charge transfer from H_2 to the metal center, giving rise to Kubas-type complexes. Moreover, a significant charge back-donation is calculated from the occupied d-orbitals of Rh and Ir to the σ^* antibonding molecular orbital of H_2.

The binding of CO is mainly due to electrostatic and charge transfer interactions. The charge is transferred from the σ-orbital of CO to the orbitals of the metal cation. For the CO binding on Rh and Ir, a significant charge back-donation from the metal to the empty π^*-orbitals of CO was calculated, which enhances the binding. The contribution of back-donation is estimated to be ~35% of the total orbital interactions for Rh and Ir, whereas a value of ~10% is estimated for the other cases.

By means of DFT calculations, we showed that the binding energies of small molecules on the open metal sites of the $M^{III}{}_3(\mu_3\text{-O})X(COO)_6$ building block (M = Al, Sc, V, Cr, Fe, Ga, Rh, In, Ir) can be tuned by changing the metal composition. We identified Rh and Ir as promising candidates for applications in H_2 storage or gas separations. This study is a baseline for future studies how the metal composition or oxidation state can affect the binding of small molecules.

■ ASSOCIATED CONTENT

Ⓢ Supporting Information

The numbering scheme (i–vi) refers to the different sections in the Supporting Information. Some sections may contain more than one table. The Supporting Information is available free of charge on the ACS Publications website at DOI: 10.1021/acs.inorgchem.5b00689.

> Tables with (i) interaction energies and (ii) harmonic frequencies calculated with different methods, (iii) CASPT2 and broken-symmetry DFT calculation on the Cr unit, (iv) detailed presentation of the EDA and the DFT-SAPT numbers, (v) plots of the main NOCVs that participate in the bonding with H_2, CO, CO_2, and (vi) density redistribution plots (PDF)
> Cartesian coordinates of all structures (PDF)

■ AUTHOR INFORMATION

Corresponding Author

*E-mail: a.mavrantonakis@jacobs-university.de.

Present Address

$^{\nabla}$Department of Chemistry, University of Minnesota, 207 Pleasant Street S.E., Minneapolis, MN 55455−0431, USA.

Notes

The authors declare no competing financial interest.

■ ACKNOWLEDGMENTS

The authors acknowledge financial support from the Deutsche Forschungsgemeinschaft (DFG) through the Priority Programme SPP 1362 (Project No. MA 532/1-1), the European Commission (ERC StG C3ENV), the Collaborative Research Center CRC/Transregio 88 (3MET, Projects B1 and C1). We also thank Prof. A. K. Powell (KIT), Prof. P. Saalfrank (University of Potsdam), Dr. G. E. Kostakis (Sussex University), Dr. N. Vankova (JUB), I. F. Akter, and M. A. Addicoat for fruitful discussions.

■ REFERENCES

(1) Lee, J.; Farha, O. K.; Roberts, J.; Scheidt, K. A.; Nguyen, S. T.; Hupp, J. T. *Chem. Soc. Rev.* **2009**, *38*, 1450−1459.

(2) Czaja, A. U.; Trukhan, N.; Müller, U. *Chem. Soc. Rev.* **2009**, *38*, 1284−1293.

(3) Murray, L. J.; Dinca, M.; Long, J. R. *Chem. Soc. Rev.* **2009**, *38*, 1294−1314.

(4) Li, J.-R.; Kuppler, R. J.; Zhou, H.-C. *Chem. Soc. Rev.* **2009**, *38*, 1477−1504.

(5) Yaghi, O. M.; O'Keeffe, M.; Ockwig, N. W.; Chae, H. K.; Eddaoudi, M.; Kim, J. *Nature* **2003**, *423*, 705−714.

(6) Panella, B.; Hirscher, M. In *Handbook of Hydrogen Storage*; Hirscher, M., Ed.; Wiley−VCH Verlag GmbH & Co. KGaA: Weinheim, Germany, 2010.

(7) Sumida, K.; Rogow, D. L.; Mason, J. A.; McDonald, T. M.; Bloch, E. D.; Herm, Z. R.; Bae, T.-H.; Long, J. R. *Chem. Rev.* **2012**, *112*, 724−781.

(8) Millward, A. R.; Yaghi, O. M. *J. Am. Chem. Soc.* **2005**, *127*, 17998−17999.

(9) Dinca, M.; Long, J. R. *Angew. Chem., Int. Ed.* **2008**, *47*, 6766−6779.

(10) Mason, J. A.; Sumida, K.; Herm, Z. R.; Krishna, R.; Long, J. R. *Energy Environ. Sci.* **2011**, *4*, 3030−3040.

(11) Fitzgerald, S. A.; Pierce, C. J.; Rowsell, J. L. C.; Bloch, E. D.; Mason, J. A. *J. Am. Chem. Soc.* **2013**, *135*, 9458−9464.

(12) Oh, H.; Savchenko, I.; Mavrandonakis, A.; Heine, T.; Hirscher, M. *ACS Nano* **2014**, *8*, 761−770.

(13) Mondloch, J. E.; Karagiaridi, O.; Farha, O. K.; Hupp, J. T. *CrystEngComm* **2013**, *15*, 9258−9264.

(14) St. Petkov, P.; Vayssilov, G. N.; Liu, J.; Shekhah, O.; Wang, Y.; Wöll, C.; Heine, T. *ChemPhysChem* **2012**, *13*, 2025−2029.

(15) Vimont, A.; Goupil, J.-M.; Lavalley, J.-C.; Daturi, M.; Surblé, S.; Serre, C.; Millange, F.; Férey, G.; Audebrand, N. *J. Am. Chem. Soc.* **2006**, *128*, 3218−3227.

(16) Garrone, E.; Otero Areán, C. *Chem. Soc. Rev.* **2005**, *34*, 846−857.

(17) Han, S. S.; Mendoza-Cortés, J. L.; Goddard, W. A., III. *Chem. Soc. Rev.* **2009**, *38*, 1460−1476.

(18) Holden, D.; Jelfs, K. E.; Cooper, A. I.; Trewin, A.; Willock, D. J. *J. Phys. Chem. C* **2012**, *116*, 16639−16651.

(19) Addicoat, M. A.; Vankova, N.; Akter, I. F.; Heine, T. *J. Chem. Theory Comput.* **2014**, *10*, 880−891.

(20) Koh, H. S.; Rana, M. K.; Hwang, J.; Siegel, D. J. *Phys. Chem. Chem. Phys.* **2013**, *15*, 4573−4581.

(21) Park, J.; Kim, H.; Han, S.; Jung, Y. *J. Phys. Chem. Lett.* **2012**, *3*, 826−829.

(22) Yu, D.; Yazaydin, O. A.; Lane, J. R.; Dietzel, P. D. C.; Snurr, R. Q. *Chem. Sci.* **2013**, *4*, 3544−3556.

(23) Lee, K.; Isley, W. C.; Dzubak, A. L.; Verma, P.; Stoneburner, S. J.; Lin, L.-C.; Howe, J. D.; Bloch, E. D.; Reed, D. a; Hudson, M. R.; Brown, C. M.; Long, J. R.; Neaton, J. B.; Smit, B.; Cramer, C. J.; Truhlar, D. G.; Gagliardi, L. *J. Am. Chem. Soc.* **2014**, *136*, 698−704.

(24) Sumida, K.; Stück, D.; Mino, L.; Chai, J.-D.; Bloch, E. D.; Zavorotynska, O.; Murray, L. J.; Dincă, M.; Chavan, S.; Bordiga, S.; Head-Gordon, M.; Long, J. R. *J. Am. Chem. Soc.* **2013**, *135*, 1083−1091.

(25) Bak, J. H.; Le, V.-D.; Kang, J.; Wei, S.-H.; Kim, Y.-H. *J. Phys. Chem. C* **2012**, *116*, 7386−7392.

(26) Canepa, P.; Arter, C. A.; Conwill, E. M.; Johnson, D. H.; Shoemaker, B. A.; Soliman, K. Z.; Thonhauser, T. *J. Mater. Chem. A* **2013**, *1*, 13597−13604.

(27) Lee, K.; Howe, J. D.; Lin, L.-C.; Smit, B.; Neaton, J. B. *Chem. Mater.* **2015**, *27*, 668−678.

(28) Suh, M. P.; Park, H. J.; Prasad, T. K.; Lim, D.-W. *Chem. Rev.* **2012**, *112*, 782−835.

(29) Getman, R. B.; Bae, Y.-S.; Wilmer, C. E.; Snurr, R. Q. *Chem. Rev.* **2012**, *112*, 703−723.

(30) Klontzas, E.; Tylianakis, E.; Froudakis, G. E. *J. Phys. Chem. Lett.* **2011**, *2*, 1824−1830.

(31) Getman, R. B.; Miller, J. H.; Wang, K.; Snurr, R. Q. *J. Phys. Chem. C* **2011**, *115*, 2066−2075.

(32) Cannon, R. D.; White, R. P. In *Progress in Inorganic Chemistry*, Vol. *36*; Lippard, S. J., Ed.; John Wiley & Sons: New York, 1988; pp 195−298.

(33) Volkringer, C.; Popov, D.; Loiseau, T.; Férey, G.; Burghammer, M.; Riekel, C.; Haouas, M.; Taulelle, F. *Chem. Mater.* **2009**, *21*, 5695−5697.

(34) Mowat, J. P. S.; Miller, S. R.; Slawin, A. M. Z.; Seymour, V. R.; Ashbrook, S. E.; Wright, P. A. *Microporous Mesoporous Mater.* **2011**, *142*, 322−333.

(35) Lieb, A.; Leclerc, H.; Devic, T.; Serre, C.; Margiolaki, I.; Mahjoubi, F.; Lee, J. S.; Vimont, A.; Daturi, M.; Chang, J.-S. *Microporous Mesoporous Mater.* **2012**, *157*, 18−23.

(36) Férey, G.; Serre, C.; Mellot-Draznieks, C.; Millange, F.; Surblé, S.; Dutour, J.; Margiolaki, I. *Angew. Chem., Int. Ed.* **2004**, *43*, 6296−6301.

(37) Horcajada, P.; Surblé, S.; Serre, C.; Hong, D.-Y.; Seo, Y.-K.; Chang, J.-S.; Grenèche, J.-M.; Margiolaki, I.; Férey, G. *Chem. Commun.* **2007**, *100*, 2820−2822.

(38) Serra-Crespo, P.; Ramos-Fernandez, E. V.; Gascon, J.; Kapteijn, F. *Chem. Mater.* **2011**, *23*, 2565−2572.

(39) Biswas, S.; Couck, S.; Grzywa, M.; Denayer, J. F. M.; Volkmer, D.; Van Der Voort, P. *Eur. J. Inorg. Chem.* **2012**, *2012*, 2481−2486.

(40) Férey, G.; Mellot-Draznieks, C.; Serre, C.; Millange, F.; Dutour, J.; Surblé, S.; Margiolaki, I. *Science* **2005**, *309*, 2040−2042.

(41) Bauer, S.; Serre, C.; Devic, T.; Horcajada, P.; Marrot, J.; Férey, G.; Stock, N. *Inorg. Chem.* **2008**, *47*, 7568−7576.

(42) Dhakshinamoorthy, A.; Alvaro, M.; Chevreau, H.; Horcajada, P.; Devic, T.; Serre, C.; Garcia, H. *Catal. Sci. Technol.* **2012**, *2*, 324−330.

(43) Liu, Y.; Eubank, J. F.; Cairns, A. J.; Eckert, J.; Kravtsov, V. C.; Luebke, R.; Eddaoudi, M. *Angew. Chem., Int. Ed.* **2007**, *46*, 3278−3283.

(44) Pang, M.; Cairns, A. J.; Liu, Y.; Belmabkhout, Y.; Zeng, H. C.; Eddaoudi, M. *J. Am. Chem. Soc.* **2012**, *134*, 13176−13179.

(45) Szilágyi, P. Á.; Serra-Crespo, P.; Dugulan, I.; Gascon, J.; Geerlings, H.; Dam, B. *CrystEngComm* **2013**, *15*, 10175−10178.

(46) Ahlrichs, R.; Bär, M.; Haser, M.; Horn, H.; Kölmel, C. *Chem. Phys. Lett.* **1989**, *162*, 165−169.

(47) *TURBOMOLE V6.5 2013*, a development of University of Karlsruhe and Forschungszentrum Karlsruhe GmbH, 1989−2007, TURBOMOLE GmbH, since 2007; available from www.turbomole.com.

(48) Deglmann, P.; Furche, F.; Ahlrichs, R. *Chem. Phys. Lett.* **2002**, *362*, 511−518.

(49) Perdew, J. P.; Ernzerhof, M.; Burke, K. *J. Chem. Phys.* **1996**, *105*, 9982−9985.

(50) Weigend, F.; Ahlrichs, R. *Phys. Chem. Chem. Phys.* **2005**, *7*, 3297−3305.

(51) Grimme, S.; Antony, J.; Ehrlich, S.; Krieg, H. *J. Chem. Phys.* **2010**, *132*, 154104.

(52) Hättig, C. *J. Chem. Phys.* **2003**, *118*, 7751−7761.

(53) Weigend, F.; Häser, M.; Patzelt, H.; Ahlrichs, R. *Chem. Phys. Lett.* **1998**, *294*, 143−152.

(54) Figgen, D.; Peterson, K. A.; Dolg, M.; Stoll, H. *J. Chem. Phys.* **2009**, *130*, 164108.

(55) Hill, J. G. *J. Chem. Phys.* **2011**, *135*, 044105.

(56) Kutzelnigg, W.; Morgan, J. D. I. *J. Chem. Phys.* **1992**, *96*, 4484−4508.

(57) Halkier, A.; Helgaker, T.; Jørgensen, P.; Klopper, W.; Koch, H.; Olsen, J.; Wilson, A. K. *Chem. Phys. Lett.* **1998**, *286*, 243−252.

(58) Martin, J. M. L.; de Oliveira, G. *J. Chem. Phys.* **1999**, *111*, 1843.

(59) Bickelhaupt, M. F.; Baerends, E. J. In *Reviews in Computational Chemistry*; Lipkowitz, K. B., Boyd, D. D., Eds.; John Wiley & Sons: New York, 2007; Vol. *15*.

(60) Nalewajski, R. F.; Mrozek, J.; Michalak, A. *Int. J. Quantum Chem.* **1997**, *61*, 589−601.

(61) Michalak, A.; DeKock, R. L.; Ziegler, T. *J. Phys. Chem. A* **2008**, *112*, 7256−7263.

(62) te Velde, G.; Bickelhaupt, F. M.; Baerends, E. J.; Fonseca Guerra, C.; van Gisbergen, S. J. A.; Snijders, J. G.; Ziegler, T. *J. Comput. Chem.* **2001**, *22*, 931−967.

(63) Heßelmann, A.; Manby, F. R. *J. Chem. Phys.* **2005**, *123*, 164116.

(64) Misquitta, A. J.; Szalewicz, K. *Chem. Phys. Lett.* **2002**, *357*, 301−306.

(65) Werner, H.-J.; Knowles, P. J.; Knizia, G.; Manby, F. R.; Schütz, M.; Celani, P.; Korona, T.; Lindh, R.; Mitrushenkov, A.; Rauhut, G.; Shamasundar, K. R.; Adler, T. B.; Amos, R. D.; Bernhardsson, A.; Berning, A.; Cooper, D. L.; Deegan, M. J. O.; Dobbyn, A. J.; Eckert, F.; Goll, E.; Hampel, C.; Hesselmann, A.; Hetzer, G.; Hrenar, T.; Jansen, G.; Köppl, C.; Liu, Y.; Lloyd, A. W.; Mata, R. A.; May, A. J.; McNicholas, S. J.; Meyer, W.; Mure, M. E.; Nicklaß, A.; O'Neill, D. P.; Palmieri, P.; Peng, D.; Pflüger, K.; Pitzer, R.; Reiher, M.; Shiozaki, T.; Stoll, H.; Stone, A. J.; Tarroni, R.; Thorsteinsson, T.; Wang, M.

MOLPRO, version 2012.1, a package of *ab initio* programs; see http://www.molpro.net.

(66) Balabanov, N. B.; Peterson, K. A. *J. Chem. Phys.* **2005**, *123*, 064107.

(67) Dunning, T. H. J. *J. Chem. Phys.* **1989**, *90*, 1007−1023.

(68) Vogiatzis, K. D.; Klopper, W.; Mavrandonakis, A.; Fink, K. *ChemPhysChem* **2011**, *12*, 3307−3319.

(69) Supronowicz, B.; Mavrandonakis, A.; Heine, T. *J. Phys. Chem. C* **2013**, *117*, 14570−14578.

(70) Hättig, C.; Klopper, W.; Köhn, A.; Tew, D. P. *Chem. Rev.* **2012**, *112*, 4−74.

(71) Kong, L.; Bischoff, F. A.; Valeev, E. F. *Chem. Rev.* **2012**, *112*, 75−107.

(72) Helgaker, T.; Klopper, W.; Tew, D. P. *Mol. Phys.* **2008**, *106*, 2107−2143.

(73) Vogiatzis, K. D.; Barnes, E. C.; Klopper, W. *Chem. Phys. Lett.* **2011**, *503*, 157−161.

(74) Vogiatzis, K. D.; Haunschild, R.; Klopper, W. *Theor. Chem. Acc.* **2014**, *133*, 1446.

(75) Vogiatzis, K. D.; Klopper, W. *Mol. Phys.* **2013**, *111*, 2299−2305.

(76) Ahnen, S.; Hehn, A.-S.; Vogiatzis, K. D.; Trachsel, M. A.; Leutwyler, S.; Klopper, W. *Chem. Phys.* **2014**, *441*, 17.

(77) Boys, S. F.; Bernardi, F. *Mol. Phys.* **1970**, *19*, 553−566.

(78) Yu, K.; Kiesling, K.; Schmidt, J. R. *J. Phys. Chem. C* **2012**, *116*, 20480−20488.

(79) Bloch, E. D.; Hudson, M. R.; Mason, J. a; Chavan, S.; Crocellà, V.; Howe, J. D.; Lee, K.; Dzubak, A. L.; Queen, W. L.; Zadrozny, J. M.; Geier, S. J.; Lin, L.-C.; Gagliardi, L.; Smit, B.; Neaton, J. B.; Bordiga, S.; Brown, C. M.; Long, J. R. *J. Am. Chem. Soc.* **2014**, *136*, 10752−10761.

(80) Reed, A. E.; Weinstock, R. B.; Weinhold, F. *J. Chem. Phys.* **1985**, *83*, 735−746.

(81) Frisch, M. J.; Trucks, G. W.; Schlegel, H. B.; Scuseria, G. E.; Robb, M. A.; Cheeseman, J. R.; Scalmani, G.; Barone, V.; Mennucci, B.; Petersson, G. A.; Nakatsuji, H.; Caricato, M.; Li, X.; Hratchian, H. P.; Izmaylov, A. F.; Bloino, J.; Zheng, G.; Sonnenberg, J. L.; Hada, M.; Ehara, M.; Toyota, K.; Fukuda, R.; Hasegawa, J.; Ishida, M.; Nakajima, T.; Honda, Y.; Kitao, O.; Nakai, H.; Vreven, T.; Montgomery, J. A., Jr.; Peralta, J. E.; Ogliaro, F.; Bearpark, M.; Heyd, J. J.; Brothers, E.; Kudin, K. N.; Staroverov, V. N.; Kobayashi, R.; Normand, J.; Raghavachari, K.; Rendell, A.; Burant, J. C.; Iyengar, S. S.; Tomasi, J.; Cossi, M.; Rega, N.; Millam, M. J.; Klene, M.; Knox, J. E.; Cross, J. B.; Bakken, V.; Adamo, C.; Jaramillo, J.; Gomperts, R.; Stratmann, R. E.; Yazyev, O.; Austin, A. J.; Cammi, R.; Pomelli, C.; Ochterski, J. W.; Martin, R. L.; Morokuma, K.; Zakrzewski, V. G.; Voth, G. A.; Salvador, P.; Dannenberg, J. J.; Dapprich, S.; Daniels, A. D.; Farkas, Ö.; Foresman, J. B.; Ortiz, J. V.; Cioslowski, J.; Fox, D. J. *Gaussian 09, Revision D.01*; Gaussian: Wallingford, CT, 2009.

(82) Ibarra, I. A.; Lin, X.; Yang, S.; Blake, A. J.; Walker, G. S.; Barnett, S. a; Allan, D. R.; Champness, N. R.; Hubberstey, P.; Schröder, M. *Chem.—Eur. J.* **2010**, *16*, 13671−13679.

(83) Areán, C. O.; Cabello, C. P.; Palomino, G. T. *Chem. Phys. Lett.* **2012**, *521*, 104−106.

(84) Palomino, G. T.; Cabello, C. P.; Areán, C. O. *Eur. J. Inorg. Chem.* **2011**, *2011*, 1703−1708.

(85) Chavan, S. M.; Zavorotynska, O.; Lamberti, C.; Bordiga, S. *Dalton Trans.* **2013**, *42*, 12586−12595.

(86) Woo, S.-J.; Lee, E.-S.; Yoon, M.; Kim, Y.-H. *Phys. Rev. Lett.* **2013**, *111*, 066102.

(87) Moellmer, J.; Celer, E. B.; Luebke, R.; Cairns, A. J.; Staudt, R.; Eddaoudi, M.; Thommes, M. *Microporous Mesoporous Mater.* **2010**, *129*, 345−353.

(88) Kubas, G. J. *Chem. Rev.* **2007**, *107*, 4152−4205.

(89) Llewellyn, P. L.; Bourrelly, S.; Serre, C.; Vimont, A.; Daturi, M.; Hamon, L.; De Weireld, G.; Chang, J.-S.; Hong, D.-Y.; Hwang, Y. K.; Jhung, S. H.; Férey, G. *Langmuir* **2008**, *24*, 7245−7250.

(90) Hong, D.-Y.; Hwang, Y. K.; Serre, C.; Férey, G.; Chang, J.-S. *Adv. Funct. Mater.* **2009**, *19*, 1537−1552.

(91) Chowdhury, P.; Bikkina, C.; Gumma, S. *J. Phys. Chem. C* **2009**, *113*, 6616−6621.

(92) Yoon, J. W.; Seo, Y.-K.; Hwang, Y. K.; Chang, J.-S.; Leclerc, H.; Wuttke, S.; Bazin, P.; Vimont, A.; Daturi, M.; Bloch, E.; Llewellyn, P. L.; Serre, C.; Horcajada, P.; Grenèche, J.-M.; Rodrigues, A. E.; Férey, G. *Angew. Chem., Int. Ed.* **2010**, *49*, 5949−5952.

(93) Bader, R. F. W. *Atoms in Molecules—A Quantum Theory*; Oxford University Press: Oxford, U.K., 1990.

(94) Volkringer, C.; Leclerc, H.; Lavalley, J.; Loiseau, T.; Férey, G.; Daturi, M.; Vimont, A. *J. Phys. Chem. C* **2012**, *116*, 5710−5719.